

Analytical Equations for Nonlinear Phase Errors and Jitter in Ring Oscillators

Shweta Srivastava and Jaijeet Roychowdhury

Abstract—In this paper, we present a simple analytical equation for capturing phase errors in 3-stage ring oscillators. The model, based on a simple but useful idealization of the ring oscillator, is provably exact for small noise perturbations. Despite its simplicity and purely analytical form, our model correctly captures the time-dependent sensitivity of oscillator phase to external perturbations. It is thus well suited for estimating both qualitative and quantitative features of ring oscillator phase response to internal noises, as well as to power, ground and substrate interference. The nonlinear nature of the model makes it suitable for predicting injection locking as well. Comparisons of the new model with existing phase models are provided, and its application for correct prediction of thermal jitter demonstrated. Requiring knowledge only of the amplitude and frequency of the oscillator, the model is ideally suited for early design exploration at the system and circuit levels.

I. INTRODUCTION

CORRECT modeling of the phase response of free-running oscillators is of great importance in the design of communication and computer systems. Phase errors caused by device or interference noise result in timing jitter and phase noise; these have a large impact on overall system functionality metrics, such as bit-error rate (BER) in communication systems and clock skew in synchronized digital systems. As a result, it is important to model phase errors as realistically as possible, from the very beginning, during architecture, system and circuit level design.

Indeed, the crucial rôle of *early design exploration* in making overall architectural decisions that best trade off performance vs cost metrics is well recognized by system designers. At the early design stage, only the sketchiest details of each block comprising the system are usually available—typically, only the broad nature or topology of a circuit block will be known. For example, during the early design process, the qualitative phase response properties of ring oscillators might be compared against those of *LC* oscillators, but the only information available about the oscillator block would be its center frequency and its desired phase noise or jitter performance. Due to the absence of concrete circuit realizations at the early design stage, using *simple generic models* of blocks that, however, capture important qualitative properties correctly, is of the utmost importance.

In this paper, we present a simple analytical equation that captures the phase response of idealized 3-stage ring oscillators (shown in Fig. 1) accurately. The simplicity of the model stems

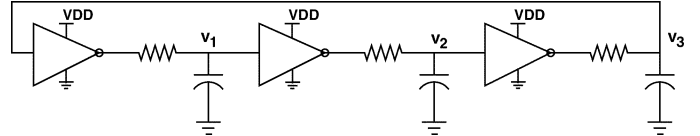


Fig. 1. Idealized ring oscillator. The inverters are assumed to switch between output levels of ± 1 , with abrupt switching at input level 0. All resistors/capacitors are assumed identical.

from its explicit dependence on only two design parameters: the amplitude (power) of the output waveforms and the oscillator's desired frequency. The equation is a single scalar nonlinear differential equation for the phase error and is amenable to further simplification and abstraction. Despite its simplicity, the model is powerful enough to capture timing jitter and phase noise due to small device and interference noises accurately. The simple analytical model can also predict injection locking. Existing oscillator phase models for early design (*e.g.*, [12], [15]), which apply a simplistic voltage-controlled oscillator (VCO)-like technique of linearly integrating noise/perturbation inputs in time to produce phase errors, do not capture these effects correctly (or at all, *e.g.*, for injection locking).

Our approach is based on a theory for nonlinear perturbation analysis developed in [2], [4], which developed a numerical procedure for finding a periodic phase-sensitivity function, termed the perturbation projection vector (PPV), of any oscillator. In this work, we apply the same rigorous theory, but in a *completely analytical* manner, employing no approximations (other than idealizing the ring oscillator system at the outset). In other words, we start by finding an exact analytical form for the steady-state of the ring oscillator, then obtain its time-varying linearization analytically, and continue to perform Floquet analysis [5] of the system, culminating in expressions for the monodromy matrix [2], [4], [5] and the PPV, analytically. The nonlinear phase macromodel is a simple scalar differential equation that employs this PPV.

Having a simple analytical expression for the PPV (as opposed to a numerical procedure for computing it) has the additional advantage of providing direct design insight into noise and perturbation properties of ring oscillators. The PPV directly captures the time-dependent sensitivity of the oscillator's phase response to any perturbations; hence plots of the PPV, together with knowledge of its scaling properties with respect to oscillation, frequency and amplitude, can guide both circuit and system design decisions without the need for system-level simulation.

Interesting features of our mathematical development include Floquet analysis of an impulsive system, a waveform-relaxation-like analytical solution technique, exact analytical eigendecompositions of integer matrices, and a form for the

Manuscript received October 20, 2004; revised May 12, 2006. This paper was recommended by Associate Editor P. K. Rajan.

The authors are with the University of Minnesota, Twin Cities, Minneapolis, MN 55455 USA (e-mail: shwetas@umn.edu; jr @umn.edu).

Digital Object Identifier 10.1109/TCSI.2007.905637

PPV that shows its explicit amplitude- and time-scaling dependence on the frequency/period. An additional curious aspect is that the number $\varphi = (1 + \sqrt{5})/2 \simeq 1.618034$, well known as the Golden Mean or Divine Proportion [6], [13], [14], emerges to be central to our exact analytical phase model.

We provide comparisons of the nonlinear equation proposed here with prior linear approaches, in particular the closed-form impulse sensitivity function (ISF) based approach of [8]. Extending what has already been shown numerically [2]–[4] and analytically for a simple oscillator in radial state space [1], we prove that for the ring oscillator, linear phase equations lead to significant qualitative and quantitative errors. In addition to providing a derivation of the analytical nonlinear phase error equation in Section II, we provide demonstrations of its application to predicting thermally-induced jitter in Section III.

II. RING OSCILLATOR: ANALYTICAL PERTURBATION ANALYSIS AND PHASE ERROR EQUATIONS

Fig. 1 depicts an idealized 3-stage ring oscillator. All resistors, capacitors and inverters are assumed identical; ideally switching inverters, with output voltages of ± 1 and input switching threshold zero, are assumed. The assumptions of symmetry and zero switching threshold are not essential, having been made simply for convenience; the key assumption, on which much of the following relies, is that of *ideal switching* of the inverters. Deviations from nonideality (especially delay-related aspects) are captured by the R and C elements outside the inverters.

The key to our novel phase macromodel is that we are able to carry out, in a completely analytical fashion, Floquet analysis [2], [5], [7] of the ring oscillator. Floquet analysis consists solving the linear periodically time-varying (LPTV) system of equations that results from linearizing the nonlinear ring oscillator about its oscillatory steady state. It is important to note, though, that while LPTV calculations are at the core of our procedure, the result of this analysis (a quantity known as the PPV [2], [4]) is used to form a *nonlinear* macromodel.¹ This nonlinearity is key to the accuracy of the analytical equation—for example, for capturing complex dynamical phenomena such as injection locking.

In this section, we obtain the new phase equation via the following steps of Floquet analysis, which we perform analytically.

- 1) First (Section II-A), we obtain the differential (1) of the ring oscillator of Fig. 1.
- 2) Next (Section II-B), we find an *exact* analytical oscillatory solution of (1), in terms of the electrical parameters of the circuit. The solution comprises analytical expressions for the time-period T of the oscillator and for the voltage waveforms at the capacitor nodes of Fig. 1.
- 3) Next (Section II-C), we find the (adjoint) linear periodically time-varying (LPTV) differential (13) that capture perturbations to the oscillator around its nominal oscillatory steady-state. (13) contains *impulsive terms* due to the abrupt switching of the inverters.

¹Indeed, extending LPTV Floquet analysis to capture nonlinear phase behavior in oscillators is the key qualitative advance of [4] over the prior pioneering work of [9] and related approaches such as [8].

- 4) Next (Section II-D), we solve (13) analytically, to obtain a general solution for any initial condition.
- 5) Using this general solution, we next calculate (Section II-E) the 3×3 *monodromy matrix* [5], [7] of the oscillator. We find that the entries of the monodromy matrix consist of only the integers 1, 4, 9 and 12. Next, we show that, surprisingly, an exact eigen-analysis of the monodromy matrix is possible *completely analytically*, resulting in expressions for all eigenvalues and eigenvectors. Furthermore, we find that all these quantities are related very simply to a single scalar number, $\varphi = (1 + \sqrt{5})/2 \simeq 1.618034$. Curiously, this quantity is the celebrated *Golden Mean* or *Divine Proportion* (e.g., [6], [13], [14]), a number well known for its significance in fields as diverse as pure mathematics, geometry, science, music and architecture. From the eigenvectors obtained, we choose the eigenvector corresponding to the oscillatory eigenvalue (*i.e.*, Floquet exponent 0).
- 6) Next (Section II-F), we use the general solution of the LPTV (13), using the oscillatory eigensolution obtained above, to find the PPV [4] analytically in (34). The analytical expression is found to be a *piecewise-exponential waveform with discontinuities*. With the PPV available analytically, it is embedded within a simple, scalar differential equation [2] to obtain the exact analytical nonlinear phase error macromodel (35).
- 7) Finally (Section II-G), we incorporate resistive noise, power rail interference and ground node interference terms into our analytical nonlinear phase error model (35).

A. Differential Equations for the Ring Oscillator

From Fig. 1, the equations of the ring oscillator may be easily derived from first principles to be

$$\dot{v}_1 = \frac{f(v_3) - v_1}{\tau}, \quad \dot{v}_2 = \frac{f(v_1) - v_2}{\tau}, \quad \dot{v}_3 = \frac{f(v_2) - v_3}{\tau} \quad (1)$$

where $f(v)$ is the ideal inverter characteristic

$$f(v) = \begin{cases} -1, & \text{if } v > 0 \\ +1, & \text{otherwise.} \end{cases} \quad (2)$$

Define $\tau = RC$.

B. Periodic Steady State

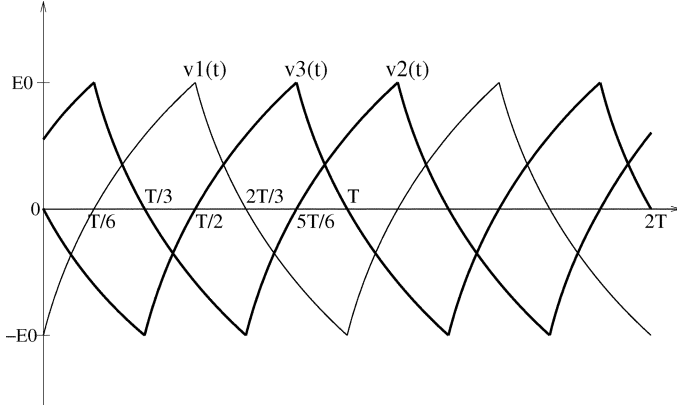
Assuming $x(t) = v_1(t)$ is T -periodic, we realize from positive-negative symmetry that

$$x(t) = -(1 + E_0)e^{-t/\tau} + 1, \quad 0 \leq t \leq \frac{T}{2} \quad (3)$$

with $x(0) = -E_0$. Requiring from symmetry that $x(T/2) = E_0$, we obtain

$$\begin{aligned} E_0 &= -(1 + E_0)e^{-T/2\tau} + 1 \\ &\Rightarrow E_0(1 + e^{-T/2\tau}) = 1 - e^{-T/2\tau} \\ &\Rightarrow E_0 = \tanh\left(\frac{T}{4\tau}\right). \end{aligned} \quad (4)$$

From delay symmetry, we have $v_2(t) = x(t - 2T/3)$ and $v_3(t) = x(t - T/3)$. From (2), it follows that the voltage at

Fig. 2. Ring oscillator steady-state waveforms: v_1, v_2, v_3 .

$v_1(t)$ will keep on increasing as long as $v_3(t) < 0$, following which it will start decreasing as soon as $v_3(t)$ rises above zero. Since $v_1(t)$ achieves its maximum at $T/2$, this implies that $v_3(t)$ has a zero crossover at $T/2$. Using these facts, we plot the steady-state waveforms for $v_1(t)$, $v_2(t)$ and $v_3(t)$, showing the zero crossover points concretely, in Fig. 2.

Hence, we have one zero crossover point at $T/6$ for $v_1(t)$.

$$0 = -(1 + E_0)e^{-T/6\tau} + 1 \Rightarrow (1 + E_0) = e^{T/6\tau}$$

$$\Rightarrow \boxed{1 + \tanh(\frac{T}{4\tau}) = e^{T/6\tau}} \quad (5)$$

we have

$$2 = e^{T/6\tau}(1 + e^{-T/2\tau}) \Rightarrow 2 - e^{T/6\tau} - e^{-2T/6\tau} = 0$$

$$\Rightarrow 2 - \varphi - \varphi^{-2} = 0, \quad \varphi = e^{T/6\tau}$$

$$\Rightarrow \varphi^3 - 2\varphi^2 + 1 = (\varphi - 1)(\varphi^2 - \varphi - 1) = 0. \quad (6)$$

Solving, we have $\varphi = (1 + \sqrt{5})/2 \simeq 1.6180339889$, the Golden Mean [6], [13]. $T = 6\ln(\varphi)\tau = 2.88727\tau$; close to the 3τ that would result from a perfect delay model. Moreover, $E_0 = \tanh(T/4\tau) = \tanh(6\ln(\varphi)/4)$.

Expanding E_0 further in terms of φ , we obtain

$$E_0 = \tanh\left(\frac{6\ln(\varphi)}{4}\right) = \frac{1 - e^{-3\ln(\varphi)}}{1 + e^{-3\ln(\varphi)}}$$

$$= \frac{1 - \varphi^{-3}}{1 + \varphi^{-3}} = \frac{\varphi^3 - 1}{\varphi^3 + 1} = \varphi - 1 \simeq 0.6180339889. \quad (7)$$

Summarizing the periodic steady-state waveform of the oscillator, we have

$$\boxed{\begin{aligned} v_1(t) &= x(t) = \begin{cases} 1 - \varphi e^{-t/\tau}, & 0 \leq t \leq \frac{T}{2} \\ -1 + \varphi e^{-(t-T/2)/\tau}, & \frac{T}{2} \leq t \leq T \end{cases} \\ v_2(t) &= x(t - \frac{2T}{3}), \quad v_3(t) = x(t - \frac{T}{3}) \end{aligned}} \quad (8)$$

with $E_0 = \varphi - 1$ and $e^{T/\tau} = \varphi^6$, where $\varphi = (1 + \sqrt{5})/2$ is the Golden Mean. Denote this periodic steady-state by $x_s(t)$, i.e., $x_s(t) = [v_1(t), v_2(t), v_3(t)]^T$. The formula above is confirmed by simulation, as shown in Fig. 3.

We next obtain an expression for the derivative of $x_s(t)$, which will be needed later

$$\dot{v}_1(t) = \dot{x}(t) = \begin{cases} \frac{1}{\tau}\varphi e^{-t/\tau}, & 0 \leq t \leq \frac{T}{2} \\ -\frac{1}{\tau}\varphi e^{-(t-T/2)/\tau}, & \frac{T}{2} \leq t \leq T \end{cases}$$

$$\dot{v}_2(t) = \dot{x}\left(t - \frac{2T}{3}\right), \quad \dot{v}_3(t) = \dot{x}\left(t - \frac{T}{3}\right). \quad (9)$$

In particular

$$\dot{x}_s(0+) = \frac{1 + E_0}{\tau}[1, \varphi^{-2}, -\varphi^{-1}]^T. \quad (10)$$

C. Time-Varying Linearized System

Next, we need to linearize (1) about the periodic steady state obtained above. Because the inverter characteristic $f(x)$ has a perfect negative step of amplitude 2 at $x = 0$, its derivative is

$$f'(x) = -2\delta(x).$$

From inspection of (1), the forward LPTV system is of the form

$$\dot{y}(t) + G(t)y(t) = 0 \quad (11)$$

where $G(t)$ is a size-3 \times 3 T -periodic matrix of the form

$$G(t) = \frac{1}{\tau} \begin{bmatrix} 1 & & -f'(v_3(t)) \\ -f'(v_1(t)) & 1 & f'(v_2(t)) \\ & -f'(v_2(t)) & 1 \end{bmatrix}$$

$$= \frac{1}{\tau} \begin{bmatrix} 1 & & 2\delta(v_3(t)) \\ 2\delta(v_1(t)) & 1 & 2\delta(v_2(t)) \\ 2\delta(v_2(t)) & 1 & 1 \end{bmatrix}. \quad (12)$$

The adjoint system is

$$\dot{y}(t) - G^T(t)y(t) = 0. \quad (13)$$

Recall from the previous section that $v_1(t) = x(t)$; $v_2(t) = x(t - (2/3)T)$; and $v_3(t) = x(t - (4/3)T) = x(t - (1/3)T)$. Hence, $v_1(t)$ has a positive zero crossing at $T/6$ and a negative zero crossing at $(2/3)T$; $v_2(t)$ has a positive zero crossing at $(5/6)T$ and a negative zero crossing at $(1/3)T$; and $v_3(t)$ has a positive zero crossing at $T/2$ and a negative zero crossing at 0. Hence, we can re-write $G(t)$ as

$$G(t) = \frac{1}{\tau} \begin{bmatrix} 1 & & G_{13}(t) \\ G_{21}(t) & 1 & G_{32}(t) \\ & G_{32}(t) & 1 \end{bmatrix} \quad (14)$$

with

$$G_{21}(t) = \frac{2}{|x'(t^*)|} \left(\delta\left(t - \frac{T}{6}\right) + \delta\left(t - \frac{2}{3}T\right) \right)$$

$$G_{32}(t) = \frac{2}{|x'(t^*)|} \left(\delta\left(t - \frac{5}{6}T\right) + \delta\left(t - \frac{1}{3}T\right) \right)$$

$$G_{13}(t) = \frac{2}{|x'(t^*)|} \left(\delta(t) + \delta\left(t - \frac{T}{2}\right) \right). \quad (15)$$

Equation (14) is valid over $t \in [0, T]$, with $G(t)$ T -periodic. $t^* = T/6$ is the point where $x(t)$ crosses zero; the slope at

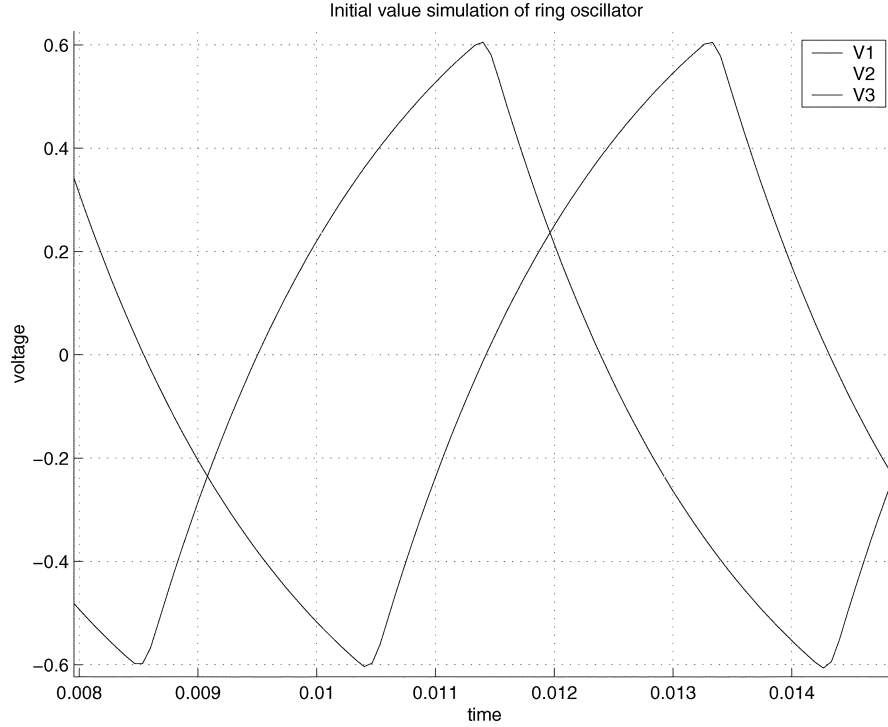


Fig. 3. Ring oscillator steady-state waveforms (simulation).

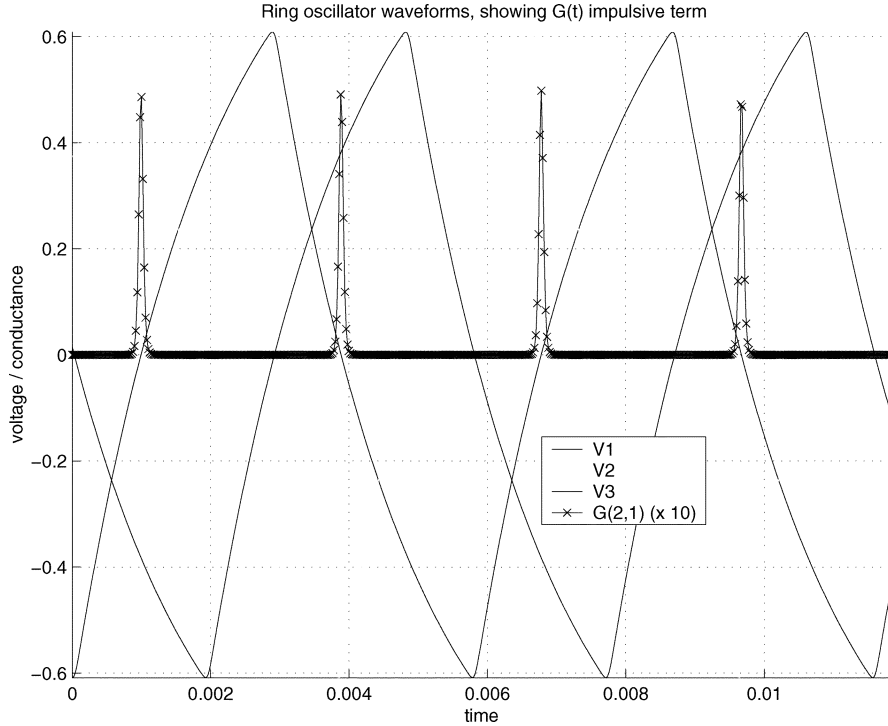


Fig. 4. $G_{2,1}(t)$ (simulation).

this point is $x'(t^*) = 1/\tau$, which follows directly from (1). Incorporating $x'(t^*)$ correctly in (14) is important for capturing the integrals of the δ -function terms, which are key metrics to be preserved. Fig. 4 depicts the impulse-like $G_{1,2}(t)$ obtained from simulation. Note that the spikes, synchronized with zero-crossings of $x(t) = v_1(t)$, are all positive, as predicted by (14).

D. Solution of the Adjoint LPTV System

Noting that

$$G^T(t) = \frac{1}{\tau} \begin{bmatrix} 1 & G_{21}(t) & G_{32}(t) \\ & 1 & \\ G_{13}(t) & & 1 \end{bmatrix} \quad (16)$$

we can expand the adjoint LPTV system $\dot{z} - G^T(t)z(t) = 0$ into individual components, and denoting $S' = 2/(\tau|x'(t^*)|) = 2$, we obtain

$$\begin{aligned}\dot{z}_1 &= \frac{z_1(\tau)}{\tau} + S' \left(\delta\left(t - \frac{T}{6}\right) z_2\left(\frac{T}{6}\right) + \delta\left(t - \frac{2}{3}T\right) z_2\left(\frac{2}{3}T\right) \right) \\ \dot{z}_2 &= \frac{z_2(\tau)}{\tau} + S' \left(\delta\left(t - \frac{1}{3}T\right) z_3\left(\frac{1}{3}T\right) + \delta\left(t - \frac{5}{6}T\right) z_3\left(\frac{5}{6}T\right) \right) \\ \dot{z}_3 &= \frac{z_3(\tau)}{\tau} + S' \left(\delta(t) z_1(0) + \delta\left(t - \frac{T}{2}\right) z_1\left(\frac{T}{2}\right) \right).\end{aligned}\quad (17)$$

The above equations can be solved analytically, using a waveform-relaxation-like approach, because of the simplicity of integrating δ functions. For given initial conditions $z_1(0)$, $z_2(0)$ and $z_3(0)$, the solution is

$$\begin{aligned}z_1(t) &= \left(z_1(0) + S' \left(e^{-T/6\tau} z_2\left(\frac{T}{6}\right) u\left(t - \frac{T}{6}\right) + e^{-2T/3\tau} z_2\left(\frac{2T}{3}\right) u\left(t - \frac{2T}{3}\right) \right) \right) e^{t/\tau} \\ z_2(t) &= \left(z_2(0) + S' \left(e^{-T/3\tau} z_3\left(\frac{T}{3}\right) u\left(t - \frac{T}{3}\right) + e^{-5T/6\tau} z_3\left(\frac{5T}{6}\right) u\left(t - \frac{5T}{6}\right) \right) \right) e^{t/\tau} \\ z_3(t) &= \left(z_3(0) + S' \left(z_1(0) u(t) + e^{-T/2\tau} z_1\left(\frac{T}{2}\right) u\left(t - \frac{T}{2}\right) \right) \right) e^{t/\tau}\end{aligned}\quad (18)$$

as can be verified by direct substitution.

Observe that the solution is not completely specified yet, since the unknown quantities $z_1(T/2)$, $z_2(T/6)$, $z_2(2T/3)$, $z_3(T/3)$ and $z_3(5T/6)$ appear on the right-hand side of (18). We can, however, solve for these in three passes through (18). In the first pass, we obtain

$$\begin{aligned}z_2\left(\frac{T}{6}\right) &= z_2(0) e^{T/6\tau} \\ z_3\left(\frac{T}{3}\right) &= (z_3(0) + S' z_1(0)) e^{T/3\tau}\end{aligned}\quad (19)$$

in the second pass, we obtain

$$\begin{aligned}z_1\left(\frac{T}{2}\right) &= (z_1(0) + S' z_2(0)) e^{T/2\tau} \\ z_2\left(\frac{2T}{3}\right) &= (z_2(0) + S' (z_3(0) + S' z_1(0))) e^{2T/3\tau}\end{aligned}\quad (20)$$

and in the third pass, we obtain

$$z_3\left(\frac{5T}{6}\right) = (z_3(0) + S' (2z_1(0) + S' z_2(0))) e^{5T/6\tau}. \quad (21)$$

Substituting (19), (20) and (21) in (18), we obtain

$$\begin{aligned}z_1(t) &= \left(z_1(0) + S' \left(z_2(0) u\left(t - \frac{T}{6}\right) + (z_2(0) + S' [z_3(0) + S' z_1(0)]) u\left(t - \frac{2T}{3}\right) \right) \right) e^{t/\tau} \\ z_2(t) &= \left(z_2(0) + S' \left([z_3(0) + S' z_1(0)] u\left(t - \frac{T}{3}\right) + [z_3(0) + S' (2z_1(0) + S' z_2(0))] u\left(t - \frac{5T}{6}\right) \right) \right) e^{t/\tau} \\ z_3(t) &= \left(z_3(0) + S' \left(z_1(0) u(t) + [z_1(0) + S' z_2(0)] u\left(t - \frac{T}{2}\right) \right) \right) e^{t/\tau}\end{aligned}\quad (22)$$

valid over $t \in [0, T]$.

E. Monodromy Matrix of the Adjoint LPTV System

To obtain the adjoint monodromy matrix, we need to evaluate the above at $t = T$, for initial conditions e_1 , e_2 and e_3 , respectively. Doing so, we obtain

$$M_A = \begin{bmatrix} 1 + S'^3 & 2S' & S'^2 \\ 3S'^2 & 1 + S'^3 & 2S' \\ 2S' & S'^2 & 1 \end{bmatrix} e^{T/\tau}. \quad (23)$$

Recalling that $S' = 2/(\tau|x'(t^*)|) = 2$ and that $e^{T/\tau} = \varphi^6$ (where $\varphi = (\sqrt{5} + 1)/2 \simeq 1.6180$, $1/\varphi = (\sqrt{5} - 1)/2$), we have

$$M_A = \underbrace{\begin{bmatrix} 9 & 4 & 4 \\ 12 & 9 & 4 \\ 4 & 4 & 1 \end{bmatrix}}_{M_{Ai}} \varphi^6. \quad (24)$$

The characteristic polynomial of M_{Ai} above is

$$p_A(\lambda) = \lambda^3 - 19\lambda^2 + 19\lambda - 1,$$

hence the eigenvalues of M_{Ai} are

$$\lambda_{1,Ai} = \varphi^{-6}, \quad \lambda_{2,Ai} = 1, \quad \lambda_{3,Ai} = \varphi^6 \quad (25)$$

resulting in eigenvalues for M_A of $\{1, \varphi^6, \varphi^{12}\}$. (Note that $\varphi^6 = 9 + 4\sqrt{5}$ and that $\varphi^{-6} = 9 - 4\sqrt{5}$). The eigendecomposition of M_{Ai} is

$$\begin{aligned}\underbrace{\begin{bmatrix} 9 & 4 & 4 \\ 12 & 9 & 4 \\ 4 & 4 & 1 \end{bmatrix}}_{M_{Ai}} \underbrace{\begin{bmatrix} -\varphi^{-1} & -1 & \varphi \\ \varphi^{-2} & 1 & \varphi^2 \\ 1 & 1 & 1 \end{bmatrix}}_V &= \underbrace{\begin{bmatrix} -\varphi^{-1} & -1 & \varphi \\ \varphi^{-2} & 1 & \varphi^2 \\ 1 & 1 & 1 \end{bmatrix}}_V \underbrace{\begin{bmatrix} \varphi^{-6} & 1 & \varphi^6 \\ & 1 & \varphi^6 \end{bmatrix}}_{\Lambda_{Ai}}.\end{aligned}\quad (26)$$

Therefore

$$M_A V = V \Lambda_A, \quad \text{with } \Lambda_A = \begin{bmatrix} 1 & \varphi^6 & \varphi^{12} \end{bmatrix}. \quad (27)$$

F. Analytical PPV and Nonlinear Phase Macromodel

We are now in a position to obtain an analytical expression for the PPV [2], [4] of the ring oscillator. Note that the eigenvector $v_1(0)$, corresponding to the periodic Floquet multiplier (eigenvalue 1), is the first column of V , or

$$V_1(0) = \varphi^{-1}[-1, \varphi^{-1}, \varphi]^T. \quad (28)$$

Applying $v_1(0)$ as the initial condition to (22), we obtain the scaled PPV function

$$\begin{aligned} V_{11}(t) &= \varphi^{-1} \left(-1 + 2 \left(\varphi^{-1} u \left(t - \frac{T}{6} \right) + (\varphi^{-1} + 2\varphi - 4) u \left(t - \frac{2T}{3} \right) \right) \right) e^{t/\tau} \\ V_{21}(t) &= \varphi^{-1} \left(\varphi^{-1} + 2 \left([\varphi - 2] u \left(t - \frac{T}{3} \right) + [\varphi + 4\varphi^{-1} - 4] u \left(t - \frac{5T}{6} \right) \right) \right) e^{t/\tau} \\ V_{31}(t) &= \varphi^{-1} (\varphi + 2(-u(t) + [-1 + 2\varphi^{-1}] u(t - \frac{T}{2}))) e^{t/\tau}. \end{aligned} \quad (29)$$

To obtain a properly scaled PPV, we need to normalize (29) against $\dot{x}_s(t)$. It suffices to calculate $K_A = V_1^T(0+) \dot{x}_s(0+)$; however, care is necessary in this calculation, since, from (29), $V_{31}(0) \neq V_{31}(0+)$. Using (10) and (29), we obtain (using $\varphi^{-2} - 2 = -\varphi$ and $E_0 = (\varphi^3 - 1)/(\varphi^3 + 1)$)

$$\begin{aligned} K_A &= V_1^T(0+) \dot{x}_s(0+) \\ &= \varphi^{-1} \frac{1+E_0}{\tau} [-1, \varphi^{-1}, \varphi - 2] \cdot [1, \varphi^{-2}, -\varphi^{-1}]^T \\ &= \varphi^{-1} \frac{1+E_0}{\tau} [-1, \varphi^{-1}, -\varphi^{-2}] \cdot [1, \varphi^{-2}, -\varphi^{-1}]^T \\ &= \varphi^{-1} \frac{1+E_0}{\tau} (-1 + 2\varphi^{-3}) = \varphi^{-1} \frac{2\varphi^3}{\tau(1+\varphi^3)} (-1 + 2\varphi^{-3}) \\ &= \varphi^{-1} \frac{2}{\tau} \left(\frac{2-\varphi^3}{1+\varphi^3} \right). \end{aligned} \quad (30)$$

We confirm correctness of K_A by also computing it as

$$\begin{aligned} K_A &= V_1^T(0-) \dot{x}_s(0-) \\ &= \varphi^{-1} \frac{1+E_0}{\tau} [-1, \varphi^{-1}, \varphi] \cdot [-\varphi^{-3}, \varphi^{-2}, -\varphi^{-1}]^T \\ &= \varphi^{-1} \frac{1+E_0}{\tau} (-1 + 2\varphi^{-3}) \end{aligned} \quad (31)$$

and noting that the result is identical to (30).

Applying the scaling constant, we obtain an analytical expression for the PPV of an ideal three-stage ring oscillator, shown in (32) at the bottom of the page.

Observe that the three components of the PPV in (32) are simply shifts of a single waveform; hence (32) can be re-written as

$$\text{PPV}(t) = \begin{bmatrix} \text{PPV}_3(t - \frac{2T}{3}) \\ \text{PPV}_3(t - \frac{T}{3}) \\ \text{PPV}_3(t) \end{bmatrix} \quad (33)$$

where (34) at the bottom of the page, holds.

With the analytical expression for the PPV (34) available, the nonlinear phase macromodel of the ring oscillator can be expressed as [2], [4]

$$\dot{\alpha}(t) = \text{PPV}^T(t + \alpha(t)) \cdot b_p(t) \quad (35)$$

where $\alpha(t)$ is the timing jitter caused by the vector perturbation $b_p(t)$ to the oscillator. The components of $b_p(t)$ represent perturbations to the individual equations of (1).

G. Incorporating Intrinsic and Interference Noise Inputs

To use (35) to analyse the ring oscillator's phase deviations due to the presence of intrinsic and interference noise from the oscillator's internal resistors, as well as from the power and ground lines, it is helpful to expand $b_p(t)$ to more explicitly represent these effects. To this end, we re-write (1) to incorporate

$$\text{PPV}(t) = \tau \frac{1+\varphi^3}{4-2\varphi^3} \left[\begin{array}{c} -1 + 2[\varphi^{-1}u(t - \frac{T}{6}) + (\varphi^{-1} + 2\varphi - 4)u(t - \frac{2T}{3})] \\ \varphi^{-1} + 2[(\varphi - 2)u(t - \frac{T}{3}) + (\varphi + 4\varphi^{-1} - 4)u(t - \frac{5T}{6})] \\ \varphi + 2[-u(t) + (-1 + 2\varphi^{-1})u(t - \frac{T}{2})] \end{array} \right] e^{t/\tau}. \quad (32)$$

$$\begin{aligned} \text{PPV}_3(t) &= \tau \frac{1+\varphi^3}{4-2\varphi^3} (\varphi + 2[-u(t) + (-1 + 2\varphi^{-1})u(t - \frac{T}{2})]) e^{t/\tau} \\ &= \frac{\tau}{2\varphi-1} \left(1 - \frac{2}{\varphi} u(t - \frac{T}{2}) \right) e^{t/\tau} \\ &= \frac{\tau}{\sqrt{5}} \left(1 - \frac{4}{\sqrt{5}+1} u(t - \frac{T}{2}) \right) e^{t/\tau} \\ &= \begin{cases} \frac{\tau}{\sqrt{5}} e^{t/\tau} & \text{if } 0 \leq t < \frac{T}{2} \\ \tau \left(\frac{2}{\sqrt{5}} - 1 \right) e^{t/\tau} & \text{if } \frac{T}{2} \leq t < T \end{cases} \\ &\simeq \tau (0.4472 - 0.5528u(t - \frac{T}{2})) e^{t/\tau}. \end{aligned} \quad (34)$$

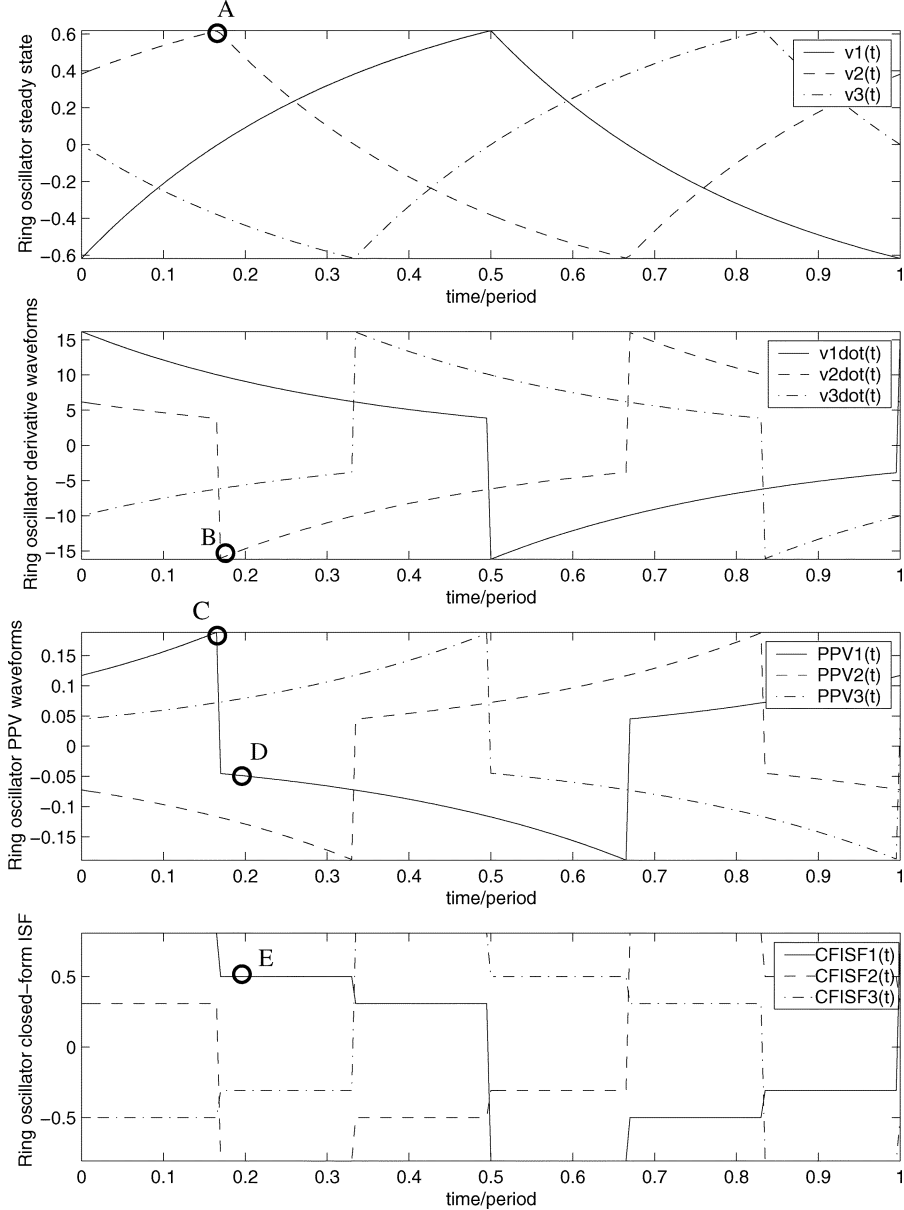


Fig. 5. Plots (from analytical expressions) of the steady-state waveform, its derivative, the PPV and the closed-form ISF [8, eq. 31] of the ideal 3-stage ring oscillator.

voltage variations $n_p(t)$ in the power supply node, voltage variations $n_g(t)$ in the ground node, and thermal noise from each of the three resistors in Fig. 1

$$\begin{aligned} \dot{v}_1 &= \frac{f(v_3) - v_1}{\tau} \\ &\quad + \frac{f_s(v_3)n_p(t) + (1 - f_s(v_3))n_g(t) + w_1(t)\sqrt{4kT\tau}}{\tau} \\ \dot{v}_2 &= \frac{f(v_1) - v_2}{\tau} \\ &\quad + \frac{f_s(v_1)n_p(t) + (1 - f_s(v_1))n_g(t) + w_2(t)\sqrt{4kT\tau}}{\tau} \\ \dot{v}_3 &= \frac{f(v_2) - v_3}{\tau} \\ &\quad + \frac{f_s(v_2)n_p(t) + (1 - f_s(v_2))n_g(t) + w_3(t)\sqrt{4kT\tau}}{\tau}. \end{aligned} \quad (36)$$

In (36) above, $f_s(x) = (1 + f(x))/2$, i.e., f_s selects 1 when the power rail is shorted through to the inverter output, and 0 when the ground rail is connected. $w_i(t)$ represent three independent stochastic white noise waveforms of identity PSD.

III. APPLICATION OF THE ANALYTICAL PHASE MODEL

A. Comparison Against Linear Phase Macromodels

Fig. 5 plots the PPV (34) for a ring oscillator with $\tau = 0.1$, together with the ring oscillator's steady-state waveform, its derivative, and the closed-form ISF from [8, eq. 31] for comparison. Several facts about the PPV are noteworthy.

The first interesting feature is that “jumps” in the PPV component of a given node (e.g., node 1, the solid lines) are not synchronized in any simple manner with the steady-state waveform or its derivative. Indeed, the PPV’s discontinuities, which

occur at its maxima/minima, take place when the oscillator's response is smooth. This indicates that any intuition about the phase sensitivity of a ring oscillator that is based on when nodes change rapidly is erroneous. Indeed, the correct intuition, derived from the PPV waveform, is that a node is most sensitive to noise and perturbations when the *next* node in the ring experiences rapid transitions. Points A, B, and C are marked in Fig. 5 to exhibit this behavior. Maxima of $PPV(v_1(t))$ (point "C" in Fig. 5) occurs when $v_2(t)$ (the next node) reaches at its maximum (point "B" in Fig. 5). It can also be noted that $v_1(t)$ is perfectly smooth at the maximal points of $PPV(v_1(t))$. Clearly, the phase sensitivity of a particular node is not related to the derivative of that node's steady-state waveform in any straightforward fashion.

It is instructive to compare the PPV with the well-known "ISFs" proposed in [8]. In this context, we first note that the (numerical) ISF [8, Appendix A], obtained via simulations of the oscillator with delta-function excitations at each perturbing input, is *not identical in general* to the "closed-form ISF" [8, Appendix B, eq. 31]. Although this fact has been established before [1]–[4], it appears to remain a point of common confusion within the community. The numerical ISF is in fact a re-discovery of the concept of oscillator phase sensitivity to perturbation that was first proposed by Kärtner [9], who also noted that it was related to the *adjoint* of the oscillator's small-signal LPTV equations. The PPV (of [2], [4] and this paper) and the numerical ISF are in fact identical to each other and to Kärtner's adjoint LPTV impulse response function² [9]. It has been established [2] that this PPV (or the numerical ISF function) is in fact the function that can correctly predict phase errors due to perturbations.

It is important to note that the correct use of the PPV/numerical ISF is within the *nonlinear* phase equation (35), not within a linear time-varying phase equation [8, eq. 11], [9]. The nonlinearity in the phase (35) is critically important for correct prediction of a variety of oscillator effects, including injection locking [10] and jitter due to power/ground interference [16]. The nonlinearity originates from the introduction of a *time shift* into Kärtner's purely LPTV model. If the voltage of a node in an oscillator is plotted against the current leaving that node, the trace of the voltage forms a closed curve (limit cycle), due to periodicity. In the presence of noise or perturbation, periodicity is lost; therefore, the trace no longer conforms to the original limit cycle. The extent of phase or time deviation from the original limit cycle depends on noise amplitude, in addition to the oscillator's steady-state characteristics. This time deviation is the reason (35) is nonlinear in $\alpha(t)$.

The normalized tangent-vector-based closed-form ISF (CF-ISF) [8, Appendix B, eq. 31] is in general not identical to the PPV, in spite of the fact that designer intuition about oscillator phase sensitivity is often (erroneously) based on this quantity. This is underscored by the dramatically different shape and magnitude of the closed-form ISF, compared to the PPV, seen in Fig. 5. While the PPV/numerical ISF scales lin-

²To avoid confusion between the numerical and closed-form ISFs, we have used the acronym PPV throughout this paper to refer to the correct quantity.

early with τ , the closed-form ISF, being normalized to 1, does not scale similarly. Phase changes from using the closed-form ISF can in fact be in the opposite direction from the correct one. For example, if a noise impulse is injected into node 1 at time about $t = (1/5)T$ (*i.e.*, 0.2 along the horizontal axis), the closed-form ISF predicts a positive phase change (point E in Fig. 5), whereas in fact, the correct phase change is in the negative direction (point D in Fig. 5) and of a different magnitude, as predicted by the PPV/numerical ISF.

We also compare the PPV with the derivative of the steady-state waveform, *i.e.*, the time-varying tangent vector to the oscillator's steady-state orbit. The tangent vector has been proposed as an approximation to the PPV/numerical ISF in [8, Appendix C] and is also sometimes used for guiding designer intuition. It can be seen from Fig. 5 that the PPV and the tangent vector are not identical—time-shifts and amplitudes are both different. From the analytical expressions, it can be seen further that the *two waveforms scale in opposite directions* with respect to the *RC* time constant τ . Hence, intuition about ring oscillator phase sensitivity that is based on the amplitude and shape of the tangent vector of the oscillator's state-space trajectory can be very misleading.

In spite of the fact that the PPV and numerical ISF are in principle identical, calculating the PPV using adjoint LPTV methods [2], [4] (as opposed to transient simulation of the oscillator with delta-function-like excitations [8]) has a number of advantages. Firstly, as we have shown in this paper, analytical expressions and design insights can result for specific circuits. Furthermore, computation of the PPV using adjoint steady-state techniques is numerically superior to direct first-principles calculation via transient simulation with delta-function inputs, for two reasons. First, adjoint calculation makes it possible to obtain phase sensitivities with respect to *all* possible inputs using a single matrix solution [4]; if direct transient simulation is used, a simulation needs to be carried out for each perturbing input, which can become tedious and expensive for large circuits. Second, transient simulation of oscillators is inherently prone to excessive numerical error, particularly for phase characteristics. In addition, transient simulation of oscillators typically involves circuit-specific heuristics, such as guesses for how long to simulate before the phase error is deemed to stabilize. For high-*Q* *LC* oscillators, this can be very many oscillation cycles, which exacerbates inefficiency and phase inaccuracy issues.

B. Jitter From Thermal Noise Perturbations

For stationary Gaussian white noise perturbations, the time-average of the square of the PPV plays a central rôle [2] in determining mean-square jitter and the shape of the oscillator's power spectral density. This quantity is identical for all three components of the PPV (33), hence it suffices to calculate its value for the third component (34). The square of the third PPV component is

$$PPV_3^2(t) = \begin{cases} \frac{\tau^2}{5} e^{2t/\tau} & \text{if } 0 \leq t < \frac{T}{2} \\ \tau^2 \frac{9-4\sqrt{5}}{5} e^{2t/\tau} & \text{if } \frac{T}{2} \leq t < T \end{cases} \quad (37)$$

while its averaged integral is

$$\begin{aligned}
 & \int_0^T \frac{\text{PPV}_3^2(t)}{T} dt \\
 &= \frac{1}{T} \left(\left[\frac{\tau^3}{10} e^{2t/\tau} \right]_0^{T/2} + \left[\frac{\tau^3}{10} (9 - 4\sqrt{5}) e^{2t/\tau} \right]_{T/2}^T \right) \\
 &= \frac{\tau^3}{10T} \left(\left[e^{2t/\tau} \right]_0^{T/2} + (9 - 4\sqrt{5}) \left[e^{2t/\tau} \right]_{T/2}^T \right) \\
 &= \frac{\tau^3}{10T} \left([e^{T/\tau} - 1] + (9 - 4\sqrt{5}) [e^{2T/\tau} - e^{T/\tau}] \right) \\
 &= \frac{3\tau^2}{5} \ln(\varphi) ([\varphi^6 - 1] + \varphi^{-6} [\varphi^{12} - \varphi^6]) \\
 &= \frac{6\tau^2}{5} \ln(\varphi) (\varphi^6 - 1) \simeq 9.7845\tau^2
 \end{aligned} \quad (38)$$

using $\varphi^{-6} = 9 - 4\sqrt{5}$ and $T/\tau = 6 \ln(\varphi)$.

The mean-square jitter increase per unit time due to resistive thermal noise from all three resistors, denoted by c , is given by [2]

$$c = 3 \times \frac{4kTR}{\tau^2} \frac{6\tau^2}{5} \ln(\varphi) (\varphi^6 - 1) \simeq 117.415 kTR \quad (39)$$

where $k = 1.3806503 \times 10^{-23}$ is Boltzmann's constant and T the ambient temperature in degrees kelvin. Note that this quantity is independent of τ .

IV. CONCLUSION AND FUTURE WORK

In this paper, we have derived a nonlinear analytical equation that correctly captures phase errors in idealized 3-stage ring oscillators. Curiously, the analytical model centers around the well-known Golden Ratio. We have applied the model to obtain a simple expression for phase noise stemming from white thermal perturbations. We have also provided comparisons with existing numerical and semi-analytical approaches for predicting phase responses in ring oscillators; further, we have clarified issues pertaining to the validity of such approaches. In addition to its intrinsic scientific novelty, the analytical nonlinear model, easily encapsulated in MATLAB, is well suited for early design exploration and simulations at the system level. We anticipate that it will find significant use not only in guiding ring oscillator design and providing insight not only into random noise, but also for supply interference, injection locking, etc.

ACKNOWLEDGMENT

The second author would like to thank G. Coram for discussions which motivated this work. He would also like to thank J. White for bringing [1] to his attention.

REFERENCES

- [1] G. Coram, "A simple 2-D oscillator to determine the correct decomposition of perturbations into amplitude and phase noise," *IEEE Trans. Circuits Syst. I, Fundam. Theory Appl.*, vol. 48, no. 7, pp. 896–898, Jul. 2001.
- [2] A. Demir, A. Mehrotra, and J. Roychowdhury, "Phase noise in oscillators: A unifying theory and numerical methods for characterization," *IEEE Trans. Circuits Syst. I, Fundam. Theory Appl.*, vol. 47, no. 5, pp. 655–674, May 2000.

- [3] A. Demir and J. Roychowdhury, *On the Validity of Orthogonally Decomposed Perturbations in Phase Noise Analysis*. Technical Memorandum. Murray Hill, NJ: Bell Laboratories, 1997.
- [4] A. Demir and J. Roychowdhury, "A reliable and efficient procedure for oscillator ppv computation, with phase noise macromodelling applications," *IEEE Trans. Comput.-Aided Design Integr. Circuits Syst.*, vol. 22, no. 2, pp. 188–197, Feb. 2003.
- [5] M. Farkas, *Periodic Motions*. New York: Springer-Verlag, 1994.
- [6] G. Meisner, The "phinest" source to the golden section, golden mean, divine proportion, Fibonacci series and φ [Online]. Available: <http://goldennumber.net>
- [7] R. Grimshaw, *Nonlinear Ordinary Differential Equations*. New York: Blackwell Scientific, 1990.
- [8] A. Hajimiri and T. H. Lee, "A general theory of phase noise in electrical oscillators," *IEEE J. Solid-State Circuits*, vol. 33, no. 2, pp. 179–194, Feb. 1998.
- [9] F. Kärtner, "Analysis of white and $f^{-\alpha}$ noise in oscillators," *Int. J. Circuit Theory Appl.*, vol. 18, pp. 485–519, 1990.
- [10] X. Lai and J. Roychowdhury, "Capturing injection locking via nonlinear phase domain macromodels," *IEEE Trans. Microw. Theory Tech.*, vol. 52, no. 9, pp. 2251–2261, Sep. 2004.
- [11] X. Lai and J. Roychowdhury, "Analytical equation for predicting injection locking in LC and ring oscillator," in *Proc. Custom Integr. Circuits Conf.*, Sep. 2005, pp. 461–464.
- [12] M. Gardner, *Phase-Lock Techniques*. New York: Wiley, 1979.
- [13] M. Livio, *The Golden Ratio: The Story of PHI, the World's Most Astonishing Number*. New York: Broadway, 2003.
- [14] M. L. Wright, The golden mean Vashti, Tallahassee, FL [Online]. Available: <http://www.vashti.net/mceinc/golden.htm>
- [15] J. L. Stensby, *Phase-Locked Loops: Theory and Applications*. Boca Raton, FL: CRC, 1997.
- [16] X. Lai and J. Roychowdhury, "Fast, accurate prediction of PLL jitter induced by power grid noise," in *Proc. IEEE CICC*, May 2004.



Shweta Srivastava received the Bachelor's degree in electrical engineering from the Indian Institute of Technology, Kanpur, India, in 2002, and is currently working towards the Master's degree in electrical engineering at the University of Minnesota.

From 2003 to 2005, she was an Associate Design Engineer with STmicroelectronics Pvt Ltd, Noida, India. Her research interests include design and simulation of mixed-signal circuits, macromodeling and fast simulation of nanotechnological and biochemical systems.



Jaijeet Roychowdhury received the Bachelor's degree in electrical engineering from the Indian Institute of Technology, Kanpur, India, in 1987, and the Ph.D. degree in electrical engineering and computer science from the University of California at Berkeley, in 1993.

From 1993 to 1995, he was with the Computer-Aided Design (CAD) Laboratory, ATT Bell Laboratories, Allentown, PA. From 1995 to 2000, he was with the Communication Sciences Research Division, Bell Laboratories, Murray Hill, NJ. From 2000 to 2001, he was with CeLight Inc. (an optical networking startup), Silver Spring, MD. Since 2001, he has been with the Electrical and Computer Engineering Department and the Digital Technology Center, University of Minnesota, Minneapolis. His professional interests include the design, analysis, and simulation of electronic, biological and mixed-domain systems. He holds ten patents.

Dr. Roychowdhury was cited for Extraordinary Achievement by Bell Laboratories in 1996. Over the years, he has authored or co-authored five best or distinguished papers at ASP-DAC, DAC, and ICCAD. He was an IEEE Circuits and Systems (IEEE CAS) Society Distinguished Lecturer during 2003–2005 and served as Program Chair of IEEE's CANDE and BMAS workshops in 2005. Currently, he serves on the Technical Program Committees of DAC, DATE, ASP-DAC, ISQED, and BMAS, on the Executive Committee of ICCAD, on the Nominations and Appointments Committee of CEDA, and as Secretary of CANDE.